A novel inverse problem in γ-rays emission imaging

Mai K Nguyen, Tuong T. Truong, Huy Duong Bui, Jean-Louis Delarbre

A NOVEL INVERSE PROBLEM IN γ-RAYS EMISSION IMAGING

MAI K. NGUYEN[a], T.T. TRUONG[b,*], H.D. BUI[c] and J.L. DELARBRE[a]

[a]*Equipes de Traitement des Images et du Signal, CNRS UMR 8051/E.N.S.E.A/Université de Cergy-Pontoise, 95014 Cergy-Pontoise, France;*
[b]*Laboratoire Physique de Théorique et Modélisation, CNRS UMR 8089/Université de Cergy-Pontoise, 95031 Cergy-Pontoise, France;*
[c]*Laboratoire de Mécanique des Solides, Ecole Polytechnique, 91128 Palaiseau, France*

This article presents a recent result on the feasibility of reconstruction of the radioactivity distribution of an object from a sequence of Compton-scattered radiation data in emission imaging. This may be regarded as a novel inverse principle as opposed to the traditional one in which the object is reconstructed only from the non-scattered rays collected at different incident directions. The new inversion procedure is described by an invertible linear integral transform which may be viewed as a generalized Radon transform and has several advantages over the old one. It improves significantly the contrast of the reconstructed image. The required data for reconstruction is easily acquired from an energy and position sensitive gamma camera under the form of scattered distribution images classified by their Compton-scattering angle. The motion of the camera in standard tomographic procedure is here no longer necessary for data taking.

Keywords: Compton-scattered radiation; γ-rays; Tomographic procedure

1. INTRODUCTION

The aim in γ-ray emission imaging is to provide a representation of the hidden inner structure of objects, without having to alter or to destroy them. This modality makes use of the penetrating power of γ rays and their interactions with matter. The object itself, after ingestion or absorption of radioactive material (radioisotope), becomes an emitting source of γ rays. Measured photon intensity distributions (hereafter called images) on a planar detector (gamma camera), along a certain number of view axis, are then exploited to reconstruct the object [2]. In this work we shall address the problem of object reconstruction in γ-ray emission imaging from an entirely new point of view.

Before getting into the crux of the subject, let us point out that in recent years γ-emission imaging has played a crucial role in many fields of application such as

*Corresponding author. E-mail: Tuong.Truong@ptm.u-cergy.fr

industrial testing (detection of defects and faults), astrophysics (imaging of galactic sources of gamma rays) and most importantly nuclear medicine, where the availability functional information on human organs (tumors, brain, heart, etc.) or on metabolism helps to provide accurate diagnostic and efficient therapy in oncology, neurology, cardiology, etc.

In principle, γ-emission imaging works with emitted photons of energy E_0. Ideally the data registered by the gamma camera as images, comes from the so-called primary (or non-scattered) photons. However this image is considerably affected by numerous factors such as absorption, noise etc. and above all the unavoidable Compton-scatter effect. Up to now, most object reconstruction methods discard the scattered photons and operate only with primary ones. Nevertheless, such reconstruction methods remain unsatisfactory, due to the very small number of detected primary photons (the noise in the image increases unacceptably with scatter elimination) and statistical fluctuations. To date the solution to the scattering problem has remained a major technical *challenge* in γ-ray imaging.

In this work, we propose an alternative approach to this problem by taking advantage of the properties of scattered photons, instead of discarding them as usually done. Actually we show that not only can these photons be used to improve the image quality, as found at first [1], but they also generate an original new imaging process. In fact, we establish a new relation between the object radioactivity density and a series of images formed by the *single*-scattered photons and *parameterized* by various angles of scattering. This relation appears as a weighted sum of conical linear integral transforms. It may be viewed as a Compound Conical Radon Transform (integral of functions on cone surfaces) [5]. Let us recall that the usual Radon transform (integrals of functions on lines or planes) is the corner stone of modern X-ray Computer Assisted Tomography (CAT). It turns out that the kernel of the new transformation, called Scatter Point Spread Function (SPSF), can be analytically computed. Moreover and most importantly, we prove that this new transformation is *invertible* and the kernel of the inverse transformation can be explicitly evaluated. These theoretical results allow the reconstruction of a 3D-object from a series of images parameterized by the angle of scattering (instead by an angle of spatial rotation). Consequently in this new imaging procedure, the recording of these images can be made without the motion of the detector as in the case of conventional tomography.

The idea of exploiting scattered radiation for imaging purposes has been proposed before, but in other contexts (e.g. Compton scattering Tomography [9] or electronic collimation in Compton camera [10]). In Compton scattering Tomography, the aim is to determine the electron density in bulk matter (instead of the radioactivity density) from Compton scattered radiation from an γ-ray external pencil beam whereas, in emission imaging with a Compton camera, the efficiency of the detector is meant to be enhanced by the collecting of all Compton scattered photons through a planar scattering medium placed ahead of the detector. Thus the use of scattered radiation in these cases is *very different* from what we propose in this article. In fact *no theoretical inversion formulas* in three dimensions have been yet established.

The article is organized as follows. By performing a physical analysis on single Compton-scattered photons we first establish, in Section 2, the so-called *imaging equation* which relates the single scattered photon flux density recorded on the detector to the radioactive volume density of the object. We then give in the next section the explicit evaluation of the kernel (SPSF) of this mapping. Next we prove the most

important property of this mapping which is the existence of an inverse mapping with an explicit computable kernel. The approach adopted here is different from the one adopted in our previous work [5] (there, an alternative treatment is given using the derivative of the imaging equation, which is free from formal divergences). Instead a direct treatment of this equation is presented and it leads to the expressions of the kernels of the Compound Conical Radon Transform and its inverse, from which an inversion theorem can be explicitly proved [7]. Conclusions and comments are given in the last section.

2. IMAGE FORMATION BY COMPTON-SCATTERED PHOTONS

2.1. Compton Scattering

Our point of view in this work is to focus on the emitted photons which undergo at least one Compton scattering and study how they may turn out to be relevant for image formation process [1].

First, we recall the relation between energy and scattering angle for the Compton-scattered photon [2]:

$$E = E_0 \frac{1}{1 + \varepsilon(1 - \cos\theta)} \tag{1}$$

where θ is the scattering angle as measured from the incident photon direction; E_0, the photon initial energy; $\varepsilon = E_0/mc^2$ and mc^2 the rest energy of the electron. Equation (1) shows that single-scattered photons have a continuous energy spectrum: $0 \leq E \leq E_0$, which is related to the scattering angle θ. But Compton scattering is also a quantum phenomena: the emergence of the scattered photon has a probability of occurrence given by the Compton differential cross-section:

$$\frac{d\sigma}{d\Omega} = \frac{r_e^2}{2} P(\theta) \tag{2}$$

where r_e is the classical radius of the electron and $P(\theta)$ the so-called Klein–Nishina probability for deflection by an angle θ:

$$P(\theta) = \frac{1}{[1 + \varepsilon(1 - \cos\theta)]^2} \left[1 + \cos^2\theta + \frac{\varepsilon^2(1 - \cos\theta)^2}{1 + \varepsilon(1 - \cos\theta)} \right]. \tag{3}$$

As a result of Compton scattering, photons leaving an emitting point source can enter the detector along the collimator's direction after one or more scattering events. However, since single-scattered photons dominate the process [8], we shall limit ourselves to these in this article.

2.2. The Imaging Equation

Thus at a given angle θ, let $\tilde{g}(\mathbf{D}, \theta)$ be the photon flux density at detector site $\mathbf{D}$. This quantity describes essentially a *secondary* emission imaging process since it is based

on secondary emission sites formed by the free electrons of the surrounding medium. In conventional image processing for γ-ray camera, they are discarded by filtering or by other correction techniques. We study now the secondary image formation process by such scattered photons.

Let $\mathbf{V}$ denote an object voxel of coordinates (ξ_V, η_V, ζ_V) and $f(\mathbf{V})$ be the object density function, defined as $f(\mathbf{V}) = f(\xi_V, \eta_V, \zeta_V)$. It represents the number of photons emitted per unit time and per unit object (or source) volume, uniformly distributed around the 4π solid angle at site $\mathbf{V}$. $f(\mathbf{V})$ is a positive function with compact support in $\mathbb{R}^3$. Thus in one given direction, making an angle θ with the vertical downward direction $O\zeta$ (see Fig. 1), the number of photons emitted in a small solid angle $d\Omega_M$ around site $\mathbf{M}$ by an elemental source volume $d\mathbf{V}$, per unit time is:

$$\frac{1}{4\pi} f(\mathbf{V})\, d\mathbf{V}\, d\Omega_M.$$

Now, by definition of the solid angle we have $d\Omega_M = d\sigma_M / MV^2$, where $d\sigma_M$ is the area element around site $\mathbf{M}$ normal to the direction VM. Consequently the flux of photons arriving at $\mathbf{M}$ in the VM direction is:

$$\frac{f(\mathbf{V})\, d\mathbf{V}}{4\pi} \frac{1}{MV^2} \exp(-\mu r)$$

where $r = VM$ and μ is the linear mean coefficient of absorption in biological tissues (i.e. organ and/or surrounding medium).

But site $\mathbf{M}$ is located either inside the studied organ or inside the surrounding biological medium, and there are $n_e(\mathbf{M})\, d\mathbf{M}$ free electrons in a small volume element $d\mathbf{M}$. Note that in general the density of electrons is not uniform. Now since $(d\sigma/d\Omega)\, d\Omega_D$

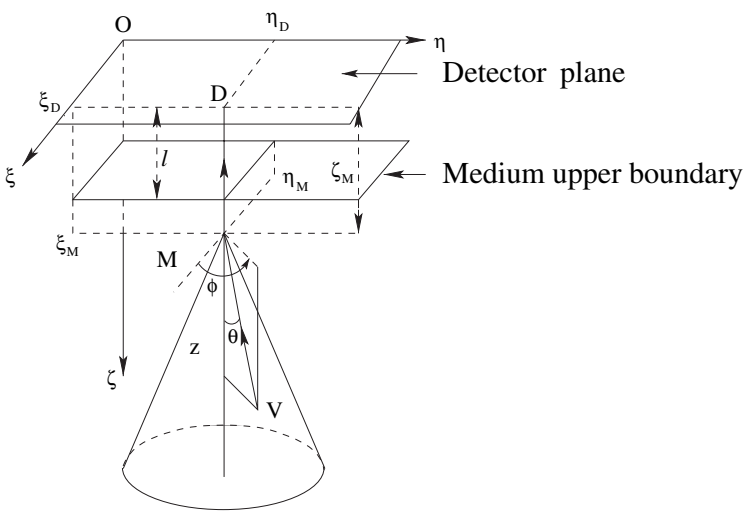

FIGURE 1 Coordinate system for the calculation of $\mathcal{T}$.

is the differential cross-section of photons scattering in the θ-direction, and since $d\Omega_D = (d\sigma_D)/(MD^2)$, the number of photons reaching a unit detector surface at $\mathbf{D}$ per unit time (after division by the area $d\sigma_D$) is the flux density recorded by the detector at site $\mathbf{D}$:

$$\frac{f(\mathbf{V})\,d\mathbf{V}}{4\pi}\,\frac{e^{-\mu r}}{MV^2}\,n_e(\mathbf{M})\,d\mathbf{M}\,\frac{r_e^2}{2}\,P(\theta)\,\frac{e^{-\mu(\zeta_M - l)}}{MD^2},$$

which depends on $d\mathbf{V}$ and $d\mathbf{M}$.

Consequently, the number of photons recorded per unit time and unit detector area at site $\mathbf{D} = (\xi_D, \eta_D)$, $\tilde{g}(\mathbf{D}, \theta)$, is due to all emitting point sources $\mathbf{V}$ situated on a cone with opening angle θ, the axis parallel to $O\zeta$ and with apex at the scattering site on the vertical line MD:

$$\begin{aligned}\tilde{g}(\mathbf{D},\theta) = &\int d\xi_M d\eta_M \frac{d\zeta_M}{\zeta_M^2}\delta(\xi_D - \xi_M)\delta(\eta_D - \eta_M)n_e(\mathbf{M})e^{-\mu(\zeta_M - l)}\\ &\times \int \frac{f(\mathbf{V})\,d\mathbf{V}}{4\pi}\frac{\delta(\mathrm{Cone})\exp(-\mu \mathrm{r})}{MV^2}\frac{r_e^2}{2}P(\theta),\end{aligned} \tag{4}$$

where δ(Cone) restricts the integration over $\mathbf{V}$ to the circular cone. In fact the cone integral has appeared first in the process of image generation in a class Compton cameras [11]. If one uses the local spherical coordinates centered at $\mathbf{M}$ in Fig. 1, we have $d\mathbf{V} = r^2 dr \sin\alpha\, d\alpha\, d\phi$ then $\delta(\mathrm{Cone}) = 1/\mathrm{r}\delta(\theta - \alpha)$. Clearly $\tilde{g}(\mathbf{D}, \theta)$ has the dimension of a photon flux through a plane (flux density) and is a positive function with compact support on $\mathbb{R}^2$.

Thus the whole process defines the integral mapping:

$$\mathcal{T} : f(\mathbf{V}) \mapsto \tilde{g}(\mathbf{D}, \theta). \tag{5}$$

Note that $\mathcal{T}$ maps a function of three variables $f(\mathbf{V})$ to $\tilde{g}(\mathbf{D}, \theta)$ which is also a function of three scalar variables, since $\mathbf{D} \in \mathbb{R}^2$ and $\theta \in \mathbb{R}$.

2.3. Explicit expressions of $\mathcal{T}$

In order to focus only on Compton effect features, other image degradations (absorption, imperfect detector) are now neglected and we set $n_e =$ constant and $\mu = 0$ for simplicity. This is a plausible hypothesis since soft biological tissues have a mass density close to that of water [2].

In Fig. 1, the measuring apparatus formed by the collimator, the detector and the photomultiplier bank is collapsed into a rectangle in the horizontal plane $O\xi\eta$. Moreover, we assume that the object under study lies below the plane $\zeta = l$, i.e. it does not touch the detector plane.

The coordinates of $\mathbf{V}$ in this system are:

$$\begin{aligned}\xi_V &= \xi_M + r\sin\theta\cos\phi,\\ \eta_V &= \eta_M + r\sin\theta\sin\phi,\\ \zeta_V &= \zeta_M + r\cos\theta,\end{aligned} \tag{6}$$

where θ is the scattering angle and ϕ the azimuthal angle of $\mathbf{V}$ with respect to the cone axis DM. The integration measure on the cone is $r\sin\theta\, d\phi\, dr$. Equation (4) after integration over ξ_M and η_M becomes our basic *imaging equation*:

$$\tilde{g}(\mathbf{D},\theta) = \tilde{K}(\theta)\int_l^\infty \frac{d\zeta_M}{\zeta_M^2}\int_0^{2\pi} d\phi \int_{0_+}^\infty \frac{dr}{r} \times f(\xi_D + r\sin\theta\cos\phi, \eta_D + r\sin\theta\sin\phi, \zeta_M + r\cos\theta), \tag{7}$$

where the factor $\tilde{K}(\theta)$ contains terms dependent on θ:

$$\tilde{K}(\theta) = \frac{n_e}{4\pi}\frac{r_e^2}{2}P(\theta)\sin\theta. \tag{8}$$

In this expression of $\tilde{g}(\mathbf{D},\theta)$, the integral on r is formally divergent near the origin since $f(\mathbf{V})$ is usually a bounded function (the activity density is everywhere finite). Mathematically, the regularization of the integral in Eq. (7) is achieved by assigning a cut-off for the integration in r; here the lower integration bound is noted 0_+. In fact in practical numerical calculations this cut-off can be easily accomplished by appropriate discretization of the integration range.

As $f(\mathbf{V})$ is of compact support, the ζ integration can be limited to the interval $l < \zeta < L$, which simplifies a great deal the numerical treatment in a real computation of the image. This ζ integral can be understood as the sum, along a vertical line, of integrals of $f(\mathbf{V})$ on cones of axis parallel to $O\zeta$, apex $\mathbf{M}$ and opening angle θ. The image of $f(\mathbf{V})$ is thus represented by a set of *conical integrals* instead of planar integrals. In this sense one may view this transformation $\mathcal{T}$ as a *Compounded Conical Radon Transform*.

We can rewrite the transformation $\mathcal{T}$ in a more suggestive form using $t = \tan\theta$, $\tilde{K}(\theta) = K(t)$ and $\tilde{g}(\mathbf{D},\theta) = g(\mathbf{D},t)$, as:

$$g(\mathbf{D},t) = \int d\mathbf{V}\, p(\mathbf{D},t|\mathbf{V}) f(\mathbf{V}). \tag{9}$$

where $p(\mathbf{D},t|\mathbf{V})$ stands for the kernel of the transformation $\mathcal{T}$:

$$p(\mathbf{D},t|\mathbf{V}) = K(t)\int_l^\infty \frac{d\zeta_M}{\zeta_M^2}\int_0^\infty \frac{dr}{r}\int_0^{2\pi} d\phi \times \delta(\xi - \xi_D - r\sin\theta\cos\phi)\,\delta(\eta - \eta_D - r\sin\theta\sin\phi)\,\delta(\zeta - \zeta_M - r\cos\theta). \tag{10}$$

Physically this kernel is also called the Point Spread Function (PSF), or image of a point source at site $\mathbf{V} = (\xi,\eta,\zeta)$. Nevertheless this image is due to *single scattered* photons rather than primary photons. This is why this kernel is called Scatter PSF (SPSF).

2.4. Computation of the SPSF kernel

Using the Fourier representation of the δ-function, and computing the integral in ζ_M as follows:

$$\int_l^\infty \frac{d\zeta_M}{\zeta_M^2}\delta(\zeta-\zeta_M-r\cos\theta)=\frac{Y(\zeta-l-r\cos\theta)}{(\zeta-r\cos\theta)^2}, \tag{11}$$

with $Y(\zeta)$ as the Heaviside unit step function. We can now represent the kernel $p(\mathbf{D},t|\mathbf{V})$ by its Fourier transform $\mathcal{P}(u,v|\zeta,t)$:

$$p(\mathbf{D},t|\mathbf{V})=\int\int du\,dv\,\mathcal{P}(u,v|\zeta,t)\exp 2i\pi[(\xi-\xi_D)u+(\eta-\eta_D)v],$$

with:

$$\mathcal{P}(u,v|\zeta,t)=2\pi K(t)\int_{0_+}^\infty \frac{dr}{r}J_0(2\pi r\sin\theta\sqrt{u^2+v^2})\frac{Y(\zeta-l-r\cos\theta)}{(\zeta-r\cos\theta)^2}. \tag{12}$$

This result shows that $\mathcal{P}(u,v|\zeta,t)$ is a function of the sole variable $\sqrt{u^2+v^2}$. We can now derive the SPSF by Fourier transformation. But in view of the rotational symmetry in Fourier space, the Fourier transform is equivalent to a Hankel transform of order zero [3]. If we introduce the following polar coordinates $(\xi-\xi_D)=\rho\cos\alpha$, $(\eta-\eta_D)=\rho\sin\alpha$ and $u=\sigma\cos\psi$, $v=\sigma\sin\psi$, then :

$$p(\mathbf{D},t|\mathbf{V})=2\pi\int_0^\infty \sigma\,d\sigma\,J_0(2\pi\rho\sigma)\,\mathcal{P}(\sigma|\zeta,t). \tag{13}$$

Now observing that $z=r\cos\theta=\rho/t$ where $t=\tan\theta$ and rearranging the expression of $\mathcal{P}(u,v|\zeta,t)$ as Hankel transform of order zero of the function (or distribution):

$$\frac{1}{z^2}\frac{Y(\zeta-z-l)}{(\zeta-z)^2},$$

we have:

$$p(\mathbf{D},t|\mathbf{V})=2\pi\int_0^\infty \sigma\,d\sigma\,J_0(2\pi\rho\sigma)\frac{K(t)}{t^2}\,2\pi\int_0^\infty \rho\,d\rho\,J_0(2\pi\rho\sigma)\frac{1}{z^2}\frac{Y(\zeta-z-l)}{(\zeta-z)^2}. \tag{14}$$

Now Hankel's identity [4]:

$$(2\pi)^2\int \sigma\,d\sigma\,J_0(2\pi\rho'\sigma)\int \rho\,d\rho\,J_0(2\pi\rho\sigma)\,f(\rho)=f(\rho'),$$

allows to conclude that for scattering angles $0<\theta<\pi/2$, $(t>0)$, the SPSF has the expression:

$$\begin{aligned} p(\mathbf{D},t|\mathbf{V}) &= p(\xi_D,\eta_D,t|\xi,\eta\zeta) \\ &= t^2K(\theta)\frac{Y(t(\zeta-l)-\rho)}{\rho^2(t\zeta-\rho)^2}. \end{aligned} \tag{15}$$

The SPSF diverges as $\rho^{-2} \to \infty$ near the origin at constant θ, when the scattering site **M** coincides with the point source **V**. It also diverges when the scattering site **M** comes to the detection site **D**, or when $t\zeta = \rho$, but this will not occur because of the limit $\zeta > l$ (recall that the object is not touching the detector plane). This kernel has also translational invariance in the detector plane:

$$p(\mathbf{D}, t|\mathbf{V}) = p((\xi - \xi_D), (\eta - \eta_D)|t, \zeta). \tag{16}$$

Now for scattering angles θ in $[\pi/2, \pi[$ or $(t < 0)$, the SPSF is:

$$p(\mathbf{D}, t|\mathbf{V}) = t^2 K(\theta) \frac{1}{\rho^2 (|t|\zeta + \rho)^2}. \tag{17}$$

There is no need to insert the Heaviside function because the scattering point lies always lower than the point source. To sum up we have the following expression for the SPSF:

$$p(\mathbf{D}, t|\mathbf{V}) = Y(t) t^2 K(\theta) \frac{Y(t(\zeta - l) - \rho)}{\rho^2 (t\zeta - \rho)^2} + Y(-t) t^2 K(\theta) \frac{1}{\rho^2 (|t|\zeta + \rho)^2}, \tag{18}$$

valid in the whole range of t values.

It is noted that the SPSF has the general shape of a "Mexican hat" for $0 < \theta < \pi/2$ and of a simple peak at the origin for other angles. Moreover, it has rotational symmetry around the projection of the point source on the detector (horizontal) plane (see Fig. 2). It is far from the Gaussian shape – a simplified form – considered in most of the actual methods of treatment of scattered radiation.

As examples illustrating our idea of taking advantage of Compton-scattered rays, we present in Fig. 3 an original object (disc of radius 6 units) and in Fig. 4 some of its scattered-ray images at various deflection angles ($\theta = 36°, 53°$, and $90°$, which correspond to energy losses of -5, -10 and -22% of the incident photon energy). These images are observed on a gamma camera of dimensions 50 units $\times$ 50 units. It is clear that the scattered-ray images carry useful information on the object structure and deserve to be used in image reconstruction. Considering them as a pure noise and discarding them as usually done is certainly not the most appropriate solution for the improvement of image quality.

Remarks At this stage a few remarks are in order. Equation (9) represents the images formed by single scattered photons. A similar equation can also be established for doubly scattered photons but the corresponding kernel is no longer simple because it is expressed as multiple integrals on different geometric variables as well as on intermediate energies. However the doubly scattered events have a very small occurrence probability which is grossly equal to the square of the Klein–Nishina probability of Eq. (3). More generally nth-order scattering events carrying the nth-power of the Klein–Nishina term have even smaller occurrence probability. Monte-Carlo studies [8] and experimental measurements [12] show that the first scattering is a dominant process compared to higher order scattering ones. As an example, in biological medium, single scattered radiation represents 36% of the total radiation against 4% of higher order scattered radiations. Thus the higher order scattering contributions

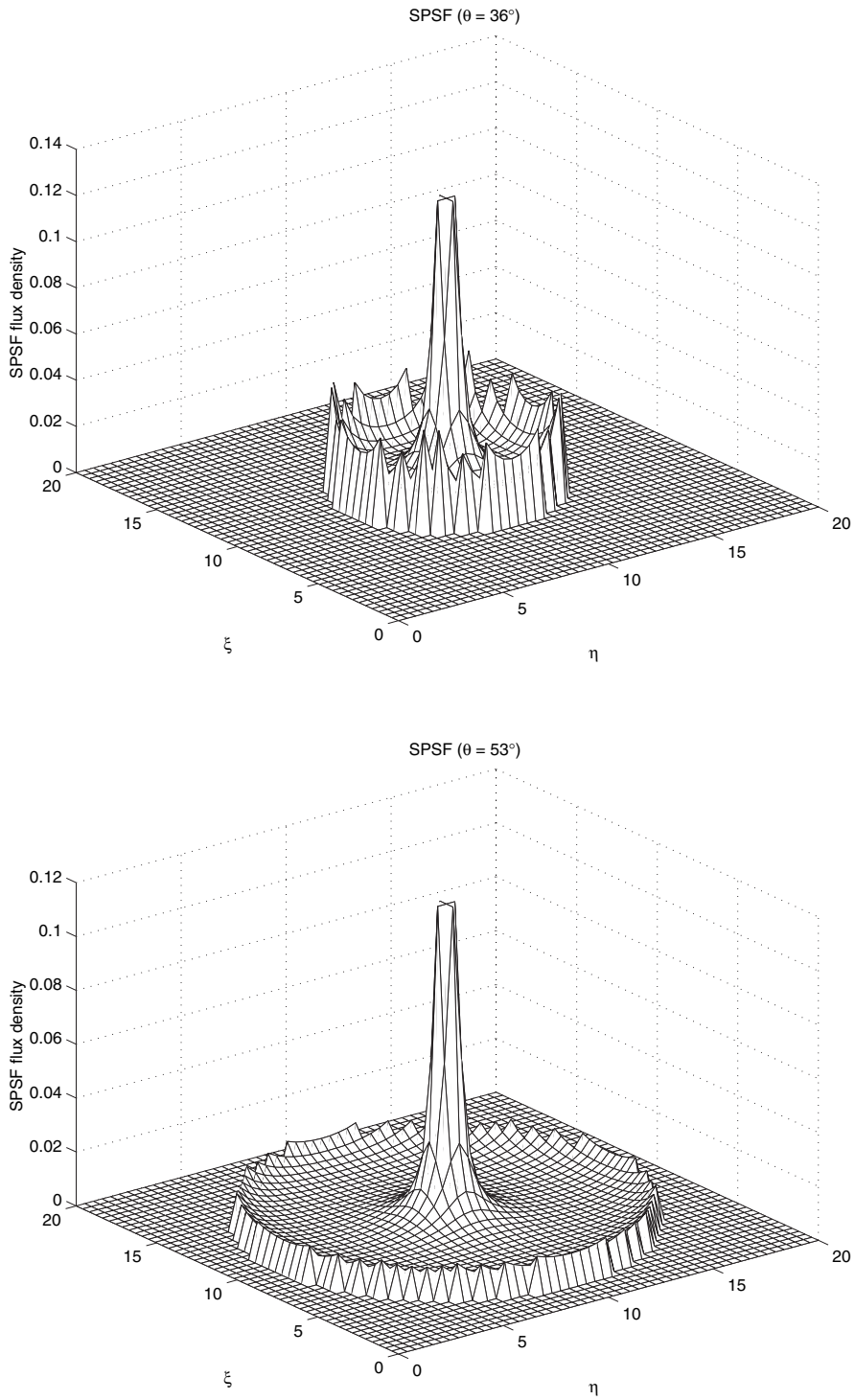

FIGURE 2 SPSF of the transform $\mathcal{T}$ at various scattering angles ($\theta = 36^\circ$, 53° and 90° respectively).

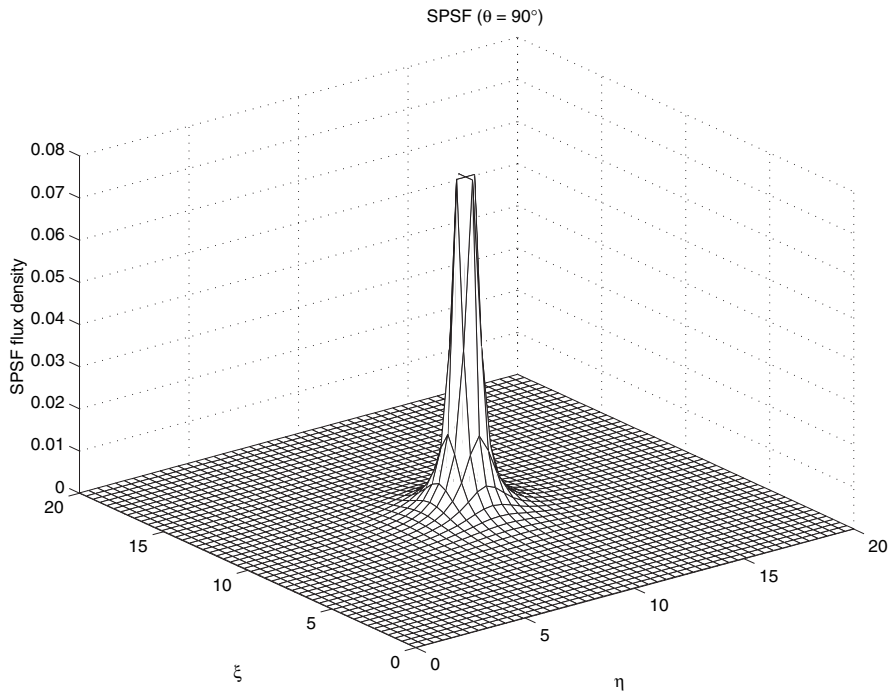

FIGURE 2 Continued.

with decreasingly low intensities can be reasonably considered as noise with respect to the dominant contributions of single scattered events. In this context, the image formation by scattered radiation considered here can be regarded as to be unique with respect to the continuous form (infinite dimension) of the integral equation (see Eq. (9)). Of course there is another problem of uniqueness related to the discretized form (finite dimension) of the integral transform, but this is an entirely different problem.

A detailed study of higher order scattering effects would give an estimate on the accuracy of the present theory based on first order scattering events (some of our preliminary results on double scattering are presented in [14]).

Next we show how the reconstruction can be performed from the single scattered rays by solving the inverse problem related to the Compound Conical Radon Transform.

3. INVERSION OF THE TRANSFORM $\mathcal{T}$

3.1. Computation of the Inverse Kernel

Having explicitly computed the kernel of the transformation $\mathcal{T}$, we show now that this transformation is *invertible* [5] and compute also the expression of the inverse kernel. Introducing the two-dimensional Fourier transform $\tilde{F}(u, v, \zeta_M; \theta)$ of $f(\mathbf{V})$ under the form:

$$\tilde{F}(u, v, \zeta_M; \theta) = \int\int d\xi_D \, d\eta_D f(\xi_D, \eta_D, \zeta_M; \theta) \exp -2i\pi(u\xi_D + v\eta_D), \tag{19}$$

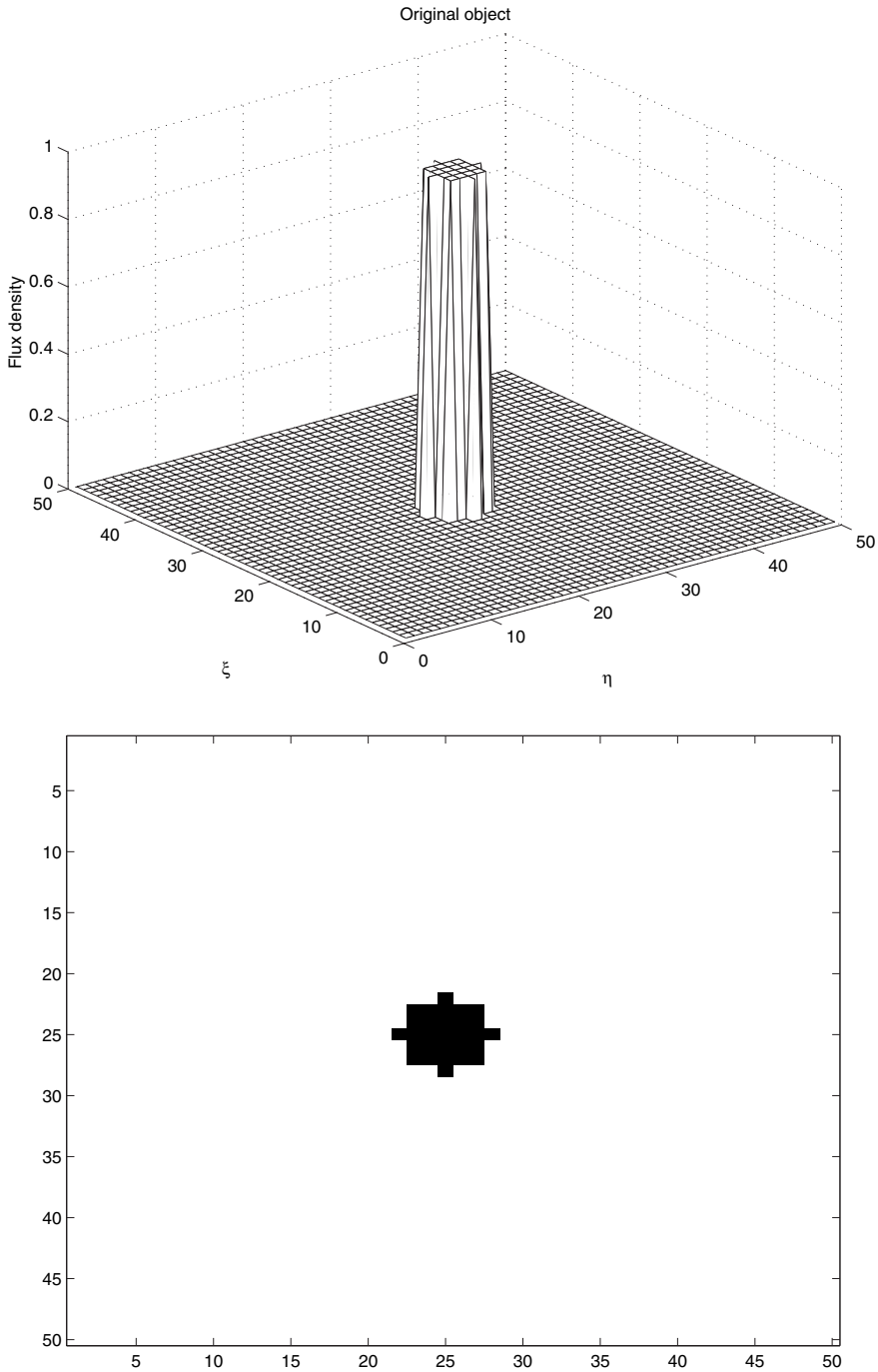

FIGURE 3 Original object (disc) and its cross-section.

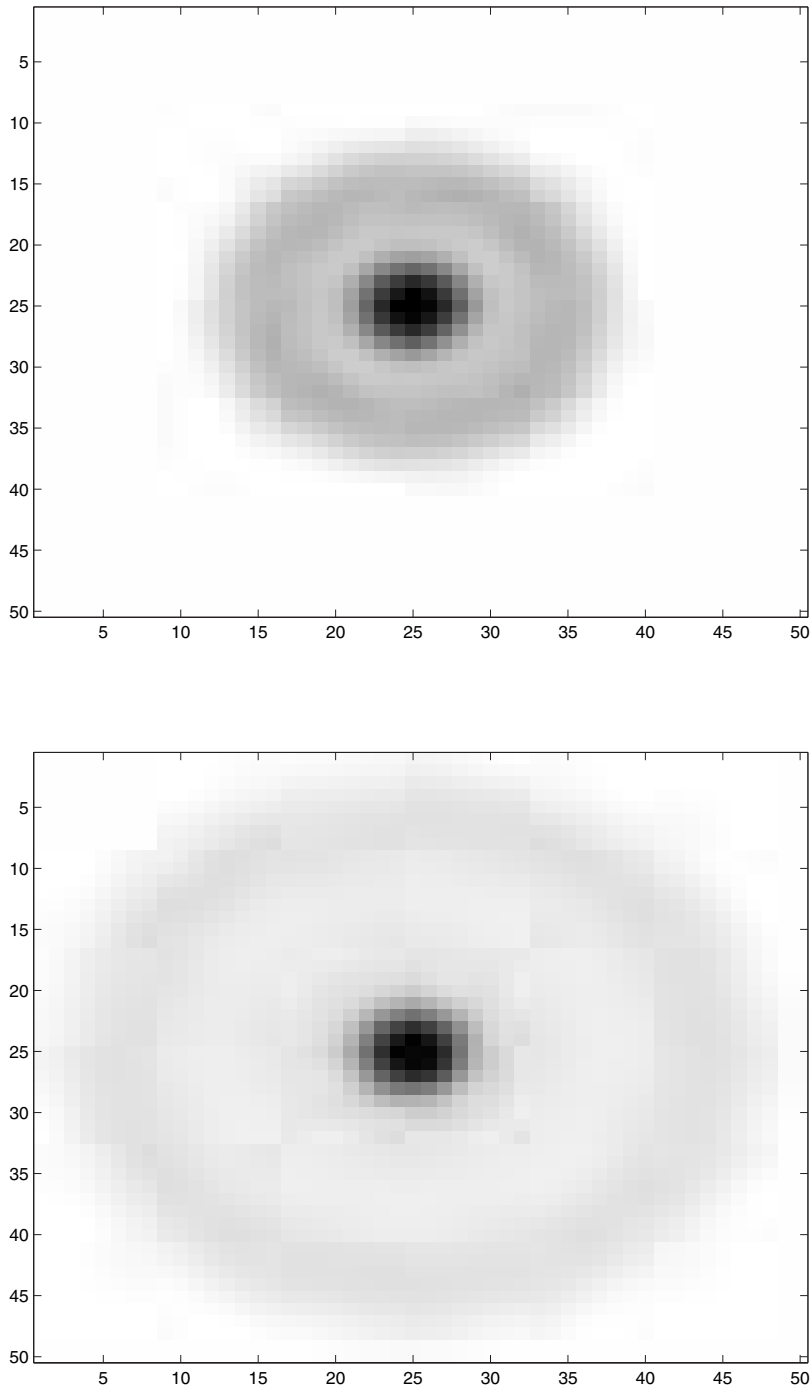

FIGURE 4 Series of secondary images parameterized by scattering angles ($\theta = 36^\circ$, 53° and 90° respectively).

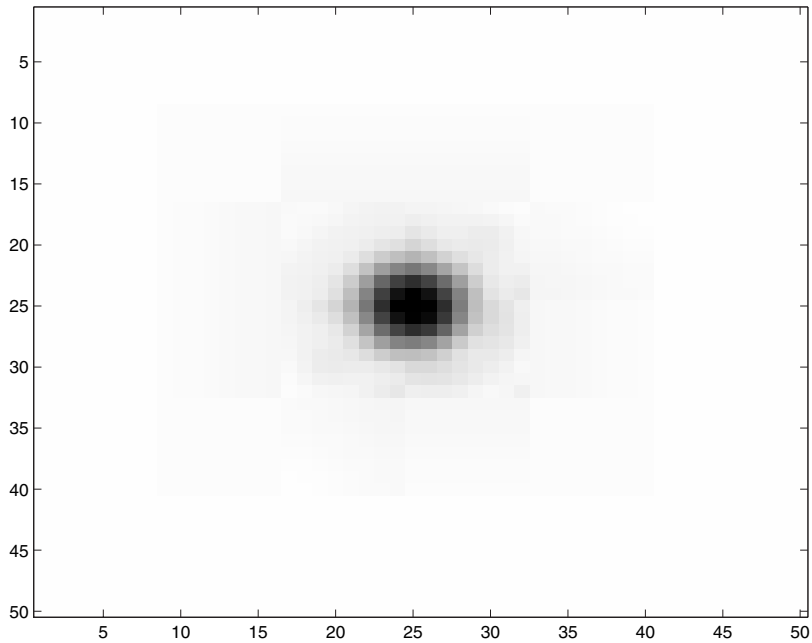

FIGURE 4 Continued.

and similarly $\tilde{G}(u, v; \theta)$ for $\tilde{g}(\mathbf{D}, \theta)$, the imaging equation (7) reads now:

$$\tilde{G}(u, v; \theta) = 2\pi\tilde{K}(\theta) \int_l^\infty \frac{d\zeta_M}{\zeta_M^2} \int_{0_+}^\infty \frac{dr}{r} \tilde{F}(u, v, \zeta_M + r\cos\theta) J_0(2\pi r \sin\theta \sqrt{u^2 + v^2}). \quad (20)$$

Now using the variables t and z defined earlier, we can cast this last equation as a Hankel transform of order zero (of course with the usual care for the lower bound of the integration):

$$G(u, v; t) = 2\pi K(t) \int_{0_+}^\infty z\, dz\, J_0(2\pi z t \sqrt{u^2 + v^2}) \frac{1}{z^2} \int_l^\infty \frac{d\zeta_M}{\zeta_M^2} F(u, v, \zeta_M + z). \quad (21)$$

The fact that we integrate z over $]0, \infty[$, means that we consider here only scattering angles $\theta \in [0, \pi/2]$ or $t > 0$ and $z > 0$.

Thus inverting "formally" the Hankel transform (the lower integration bound is considered as to be 0), one obtains:

$$\frac{1}{z^2} \int_l^\infty \frac{d\zeta_M}{\zeta_M^2} F(u, v, \zeta_M + z) = 2\pi(u^2 + v^2) \int_{0_+}^\infty t\, dt\, J_0(2\pi z t \sqrt{u^2 + v^2}) \frac{G(u, v; t)}{K(t)}. \quad (22)$$

In the other range of θ, i.e. $\theta \in [\pi/2, \pi[$ we have $t < 0$ and $z < 0$, the previous relation becomes:

$$\frac{1}{z'^2} \int_l^\infty \frac{d\zeta_M}{\zeta_M^2} F(u, v, \zeta_M - z') = 2\pi(u^2 + v^2) \int_{0_+}^\infty t'\, dt'\, J_0(2\pi z' t' \sqrt{u^2 + v^2}) \frac{G(u, v; -t')}{K(-t')}, \quad (23)$$

where $z = -z'$ and $t = -t'$ with $z' > 0$ and $t' > 0$. We can put the two inverse cases together in a single formula, valid for all t, as follows:

$$\int_l^\infty \frac{d\zeta_M}{\zeta_M^2} F(u, v, \zeta_M + z) = 2\pi(u^2 + v^2)\, z^2 \int_{0_+}^\infty t\, dt\, J_0(2\pi|z|t\sqrt{u^2 + v^2}) \times \left[Y(z) \frac{G(u, v; t)}{K(t)} + Y(-z) \frac{G(u, v; -t)}{K(-t)} \right]. \tag{24}$$

Now the left hand side of the previous equation can be put under an alternative form using Fourier analysis:

$$\int_l^\infty \frac{d\zeta_M}{\zeta_M^2} F(u, v, \zeta_M + z) = \int_{-\infty}^\infty dw\, \mathcal{J}_l(w) \bar{F}(u, v, w) \exp[-2i\pi\, w(l + z)], \tag{25}$$

where $\bar{F}(u, v, w)$ is the three-dimensional Fourier transform of $f(\mathbf{V})$, $\mathcal{J}_l$ the Fourier transform of $Y(s)(s + l)^{-2}$ is given in Fourier tables as:

$$\mathcal{J}_l(w) = 2i\pi w \left\{ e^{2i\pi l w} [Ci(2\pi l|w|) - i\, \epsilon(w)\, Si(2\pi l|w|)] - \frac{i}{2\pi w l} \right\}, \tag{26}$$

here the variable s is related to ζ_M by $\zeta_M = (s + l)$ and $\epsilon(w)$ is the sign function of w. The variable $(z + l)$ may take now any value in $\mathcal{R}$.

To extract $\bar{F}(u, v, w)$, we make an inverse Fourier transform on the last form of the imaging Eq. (24):

$$\bar{F}(u, v, w) = \frac{1}{\mathcal{J}_l(w)} \int_{-\infty}^\infty dz\, e^{2i\pi w(z+l)}\, (u^2 + v^2)\, z^2 2\pi \int_{0_+}^\infty t\, dt\, J_0(2\pi|z|t\sqrt{u^2 + v^2} \times \left[Y(z) \frac{G(u, v; t)}{K(t)} + Y(-z) \frac{G(u, v; -t)}{K(-t)} \right]. \tag{27}$$

Finally, performing the three-dimensional Fourier transform on the previous Eq. (27) and reexpressing $G(u, v; t)$ as inverse two dimensional Fourier transform of $g(\mathbf{D}, t)$, the inverse transform $\mathcal{T}^{-1}$ can be put as:

$$f(\mathbf{V}) = \int \int_{-\infty}^\infty d\mathbf{D} \int_0^\infty dt\, p^{-1}(\mathbf{V}|\mathbf{D}, t)\, g(\mathbf{D}, t), \tag{28}$$

with the inverse kernel:

$$p^{-1}(\mathbf{V}|\mathbf{D}, t) = \int \int_{-\infty}^\infty du\, dv\, e^{2i\pi[u(\xi - \xi_D) + v(\eta - \eta_D)]} (u^2 + v^2) \times 2\pi \int_{-\infty}^\infty z\, dz\, J_0(2\pi|z|t\sqrt{u^2 + v^2})\, z\, H_l(\zeta + z + l)\, t\mathcal{K}_t, \tag{29}$$

where:

$$\int_{-\infty}^{\infty} dw\ \exp[2i\pi(\zeta + z + l)w]\ \frac{1}{\mathcal{J}_l(w)} = H_l(\zeta + z + l),$$

and $\mathcal{K}_t$ is a discrete linear operator defined by:

$$\mathcal{K}_t\, g(\mathbf{D}, t) = \left[Y(z)\frac{g(\mathbf{D}, t)}{K(t)} + Y(-z)\frac{g(\mathbf{D}, -t)}{K(-t)} \right].$$

Now by splitting up the integration range of z into two parts: $]-\infty, 0]$ and $[0, \infty[$ and taking care of the action of $\mathcal{K}_t$, we obtain a new form of the inversion formula:

$$\begin{aligned} f(\mathbf{V}) = &\int_{-\infty}^{\infty} d\xi_D \int_{-\infty}^{\infty} d\eta_D \int_0^{\infty} dt \int\int_{-\infty}^{\infty} du\, dv\, e^{2i\pi[u(\xi-\xi_D)+v(\eta-\eta_D)]}(u^2+v^2) \\ &\times 2\pi \int_0^{\infty} z\, dz\, J_0(2\pi|z|t\sqrt{u^2+v^2})\, z \left[H_l(\zeta + z + l)\frac{tg(\mathbf{D}, t)}{K(t)} + H_l(\zeta - z + l)\frac{tg(\mathbf{D}, -t)}{K(-t)} \right]. \end{aligned} \tag{30}$$

The integration on z in Eq. (30) may be viewed as a Hankel transform of the function $zH_l(\zeta \pm z + l)$:

$$2\pi \int_0^{\infty} z\, dz\, J_0(2\pi|z|t\sqrt{u^2+v^2})\, z\, H_l(\zeta \pm z + l) = \mathcal{H}^{\pm}(\zeta + l, t\sqrt{u^2+v^2}). \tag{31}$$

Then the two-dimensional Fourier transform of the kernel $p^{-1}(\mathbf{V}|\mathbf{D}, t)$ reads simply:

$$\mathcal{P}^{-1}(u, v|\zeta, t) = (u^2+v^2)\mathcal{K}_t(u^2+v^2, \zeta), \tag{32}$$

where $\mathcal{K}_t(u^2+v^2, \zeta)$ is a linear discrete operator defined by:

$$\mathcal{K}_t(u^2+v^2, \zeta)g(\mathbf{D}, t) = \left[\frac{t\mathcal{H}^{+}(\zeta + l, t\sqrt{u^2+v^2})}{K(t)} g(\mathbf{D}, t) + \frac{t\mathcal{H}^{-}(\zeta + l, t\sqrt{u^2+v^2})}{K(-t)} g(\mathbf{D}, -t) \right]. \tag{33}$$

The integration over t in Eq. (30) has the meaning that one must use a *series of images labelled by the scattering angle* θ to reconstruct the object. Thus this angle θ plays the role of a scanning parameter (spatial rotation angle) in a standard tomographic imaging procedure. This inverse kernel has obviously translational invariance in the detector plane. Let $\mathbf{S}$ be the projection of $\mathbf{V}$ on the detector plane, then we may write:

$$\begin{aligned} p^{-1}(\mathbf{V}|\mathbf{D}, t) &= p^{-1}(\mathbf{S}, \zeta|\mathbf{D}, t) = p^{-1}(\mathbf{DS}|\zeta, t) \\ &= \int\int_{-\infty}^{\infty} du\, dv\, e^{2i\pi[u(\xi-\xi_D)+v(\eta-\eta_D)]}(u^2+v^2)\mathcal{K}_t(u^2+v^2, \zeta). \end{aligned} \tag{34}$$

3.2. Proof of the Inversion Relation

In this section we shall give the proof of:

$$\int d\mathbf{D}\, dt\, p^{-1}(\mathbf{V}|\mathbf{D}, t)p^*(\mathbf{D}, t|\mathbf{V}') = \delta(\mathbf{V} - \mathbf{V}') \tag{35}$$

where the star means complex conjugate. By going to the two dimensional Fourier transform, the left hand side can be written as:

$$\int_0^\infty dt \int\int_{-\infty}^{\infty} du\, dv\, e^{2i\pi[u(\xi-\xi')+v(\eta-\eta')]}\mathcal{P}^{-1}(u, v|\zeta, t)\mathcal{P}(u, v|\zeta', t). \tag{36}$$

In order to perform this calculation an alternative form for $\mathcal{P}(u, v|\zeta', t)$ using a Fourier representation is needed. We first express:

$$\frac{Y(\zeta' - z' - l)}{(\zeta' - z')^2} = \int_{-\infty}^{\infty} dw'\, \mathcal{J}_l(w')e^{2i\pi(\zeta'-z'-l)w'}, \tag{37}$$

and insert it in:

$$\mathcal{P}(u, v|\zeta, t) = 2\pi K(t) \int_{0_+}^{\infty} \frac{dz'}{z'} J_0(2\pi z' t\sqrt{u^2 + v^2}) \int_{-\infty}^{\infty} dw'\, \mathcal{J}_l(w')e^{2i\pi(\zeta'-z'-l)w'}. \tag{38}$$

Now using the expression of $\mathcal{P}^{-1}(u, v|\zeta, t)$ in Eq. (32) and the previous form of $\mathcal{P}(u, v|\zeta', t)$ we can perform the t integration in:

$$\begin{aligned}
&\int_0^\infty dt\, \mathcal{P}^{-1}(u, v|\zeta, t)\mathcal{P}(u, v|\zeta', t) \\
&\quad = 2\pi \int_0^\infty dt\, K(t) \int_{0_+}^{\infty} \frac{dz'}{z'} J_0(2\pi z' t\sqrt{u^2 + v^2}) \\
&\qquad \times \int_{-\infty}^{\infty} dw'\, \mathcal{J}_l(w')e^{2i\pi(\zeta'-z'-l)w'} 2\pi \frac{t}{K(t)}(u^2 + v^2) \int_{-\infty}^{\infty} z\, dz\, J_0(2\pi|z|t\sqrt{u^2 + v^2})\, z \\
&\qquad \times \int_{-\infty}^{\infty} dw \frac{e^{2i\pi(\zeta+z+l)w}}{\mathcal{J}_l(w)},
\end{aligned} \tag{39}$$

and we see here that the $K(t)$ factors cancel out. The integration on t can be carried out using the Bessel identity:

$$\int_0^\infty \sigma\, d\sigma\, J_0(z'\sigma)J_0(z\sigma) = \frac{1}{z'}\delta(z - z'). \tag{40}$$

Then after integration over dz for $t > 0$ and also $z > 0$, we get:

$$\int_0^\infty dt\mathcal{P}^{-1}(u,v|\zeta,t)\mathcal{P}(u,v|\zeta',t) = \int_0^\infty \frac{dz'}{z'}\int_{-\infty}^\infty dw'\,\mathcal{J}_l(w')e^{2i\pi(\zeta'-z'-l)w'} \times \frac{1}{z'}\delta(z-z')\int_{-\infty}^\infty z^2\,dz\int_{-\infty}^\infty dw\,\frac{1}{\mathcal{J}_l(w)}\,e^{2i\pi(\zeta+z+l)w}. \quad (41)$$

The integration with respect to z' removes all the z factors, and we are left with:

$$\int_0^\infty dt\mathcal{P}^{-1}(u,v|\zeta,t)\mathcal{P}(u,v|\zeta',t) = \int_{-\infty}^\infty dz\,e^{2i\pi(w-w')}\int_{-\infty}^\infty dw'\,\mathcal{J}_l(w')e^{2i\pi w'(\zeta'-l)}$$
$$\int_{-\infty}^\infty dw\,\frac{1}{\mathcal{J}_l(w)}\,e^{2i\pi w(\zeta+l)} = \int\int_{-\infty}^\infty dw\,dw'\mathcal{J}_l(w')\frac{\delta(w-w')}{\mathcal{J}_l(w)}e^{2i\pi w'(\zeta'-l)}\,e^{2i\pi w(\zeta+l)}$$
$$= \int_{-\infty}^\infty dw\,e^{2i\pi(\zeta'-\zeta)w} = \delta(\zeta'-\zeta). \quad (42)$$

The remaining integrations over du and dv yield obviously $\delta(\xi'-\xi)\,\delta(\eta'-\eta)$. The product of the kernels $p^{-1}(\mathbf{V}|\mathbf{D},t)$ with the SPSF kernel $p(\mathbf{D},t|\mathbf{V})$ is thus the identity [7].

3.2. Numerical Results

As an illustration of the inversion procedure discussed in the previous section, we present some numerical simulations which have been carried out with the following working conditions:

- the used γ-detector is a SPECT (Single Photon Emission Computed Tomography) camera. It has discretized dimensions N length units $\times N$ length units. We have chosen $N = 16$ to keep the volume of calculations reasonable.
- the scattering medium is represented by a cube of dimensions $N \times N \times N$,
- the electron density in biological medium is $n_e = 3.5 \times 10^{23}$ electrons/cm^3,
- the radio pharmaceutical employed is Technecium 99 with an activity density 2.2×10^{-2} Ci/cm^3,
- the acquisition time per image is 0.1 s,
- the 3D original object (cylinder of height 6 units) is placed at the center of the scattering medium (cube),
- the distance from camera to the upper face of the scattering medium cube is $l = 200$ units.

Figure 5(a) represents the original object. Figure 5(b) shows the series of images of the object at various scattering angles θ ($5^\circ < \theta < 175^\circ$). These images, respectively without and with Poisson emission noise, observed on the detector, are shown respectively in Fig. 6(a) and (b).

In Fig. 7(a) is the reconstructed object in the absence of noise with a RMSE = 1.2% whereas in Fig. 7(b) the reconstruction is realized in the presence of noise ($S/N = 9.7$ dB) with a RMSE = 8.9%, which is perfectly reasonable. We observe a good performance of the Compound Conical Radon Transformation for modelling the new imaging process.

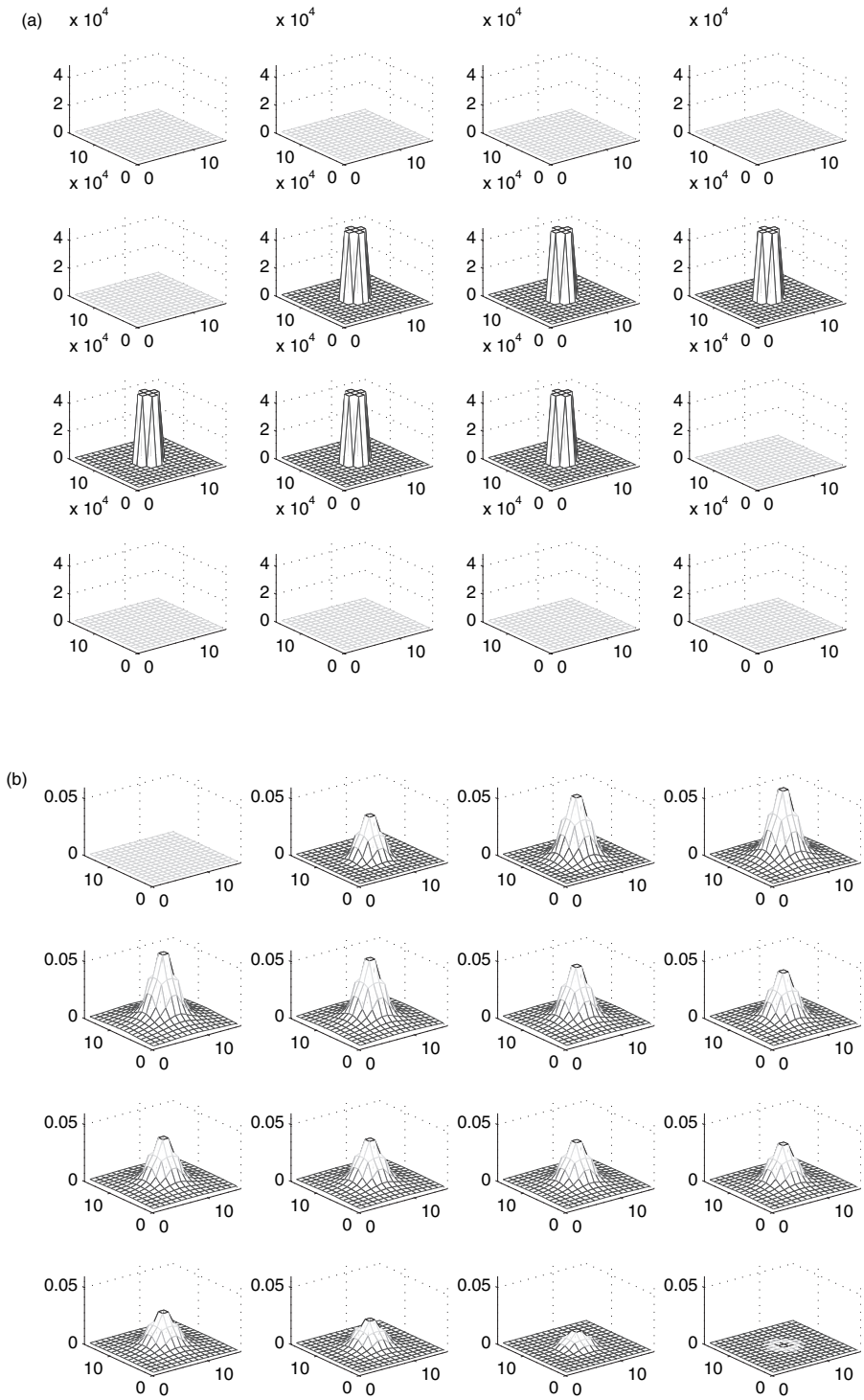

FIGURE 5 (a) Original object (cylinder) in a cube formed by 16 planes; (b) series of images parameterized by the angle of scattering θ ($5^\circ < \theta < 175^\circ$).

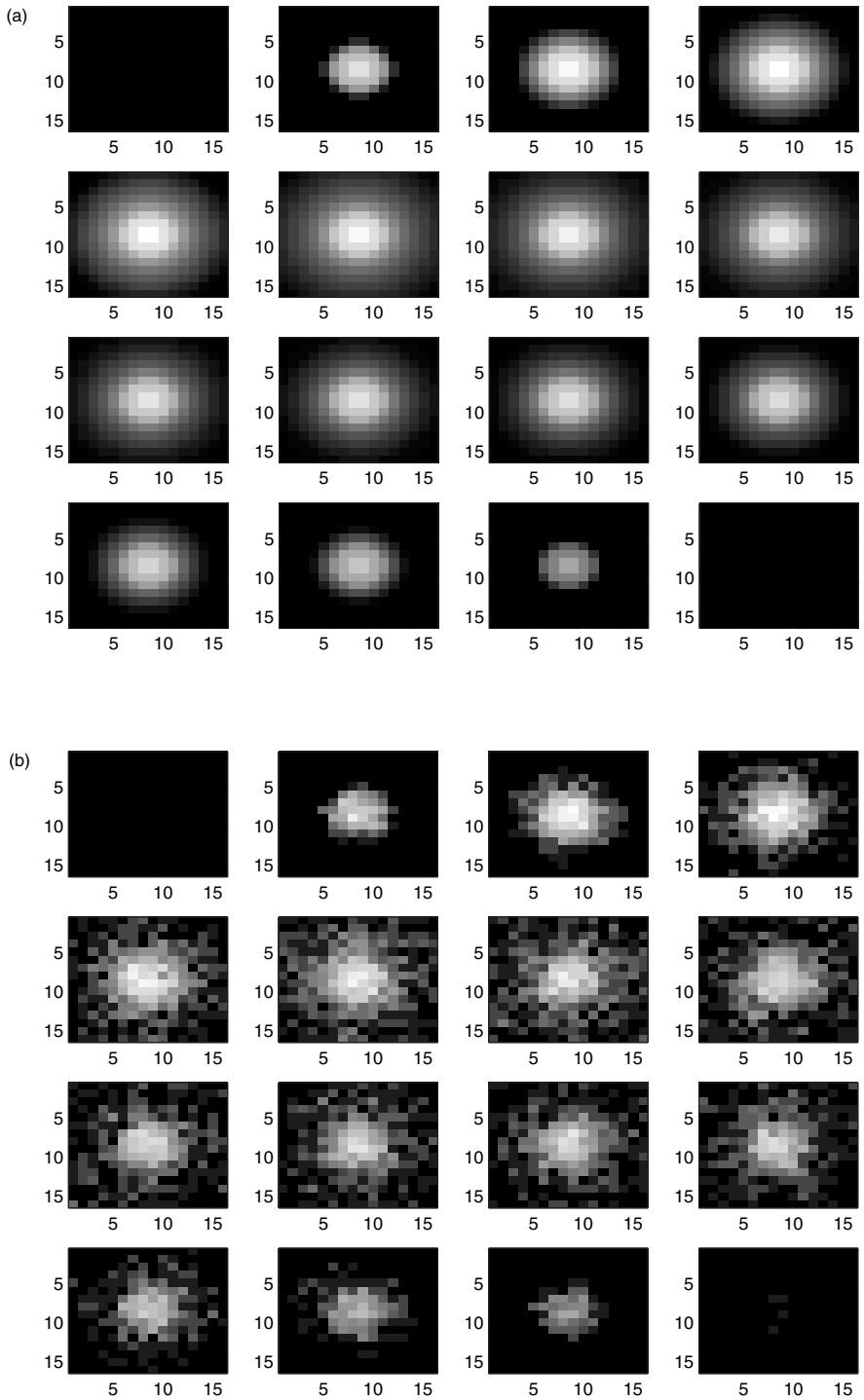

FIGURE 6 (a) Series of images without noise observed on the γ-camera; (b) series of images with noise observed on the γ-camera ($S/N = 9.7$ dB).

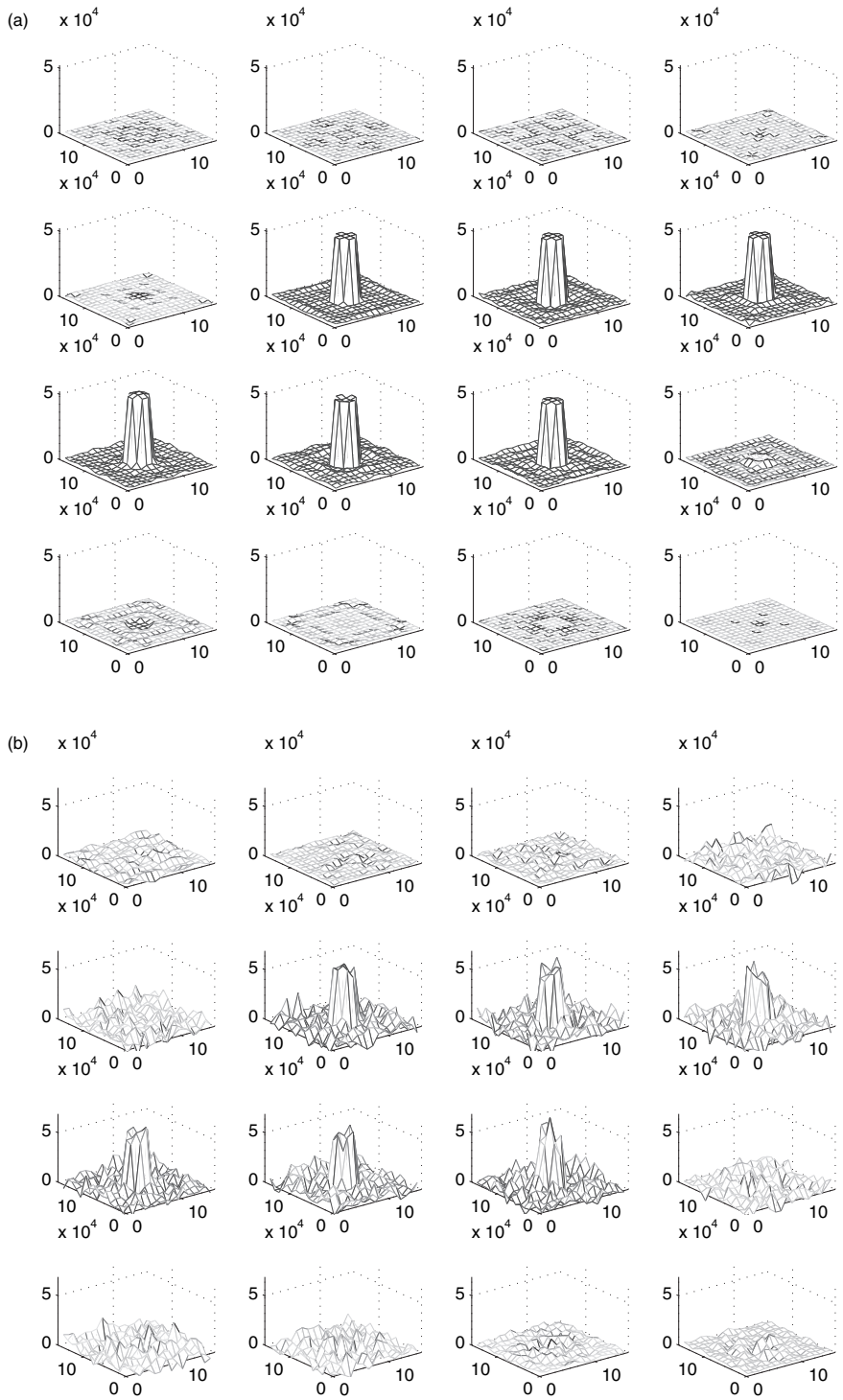

FIGURE 7 (a) Reconstructed object in the absence of noise (RMSE = 1.2%); (b) reconstructed object in the presence of noise (with $S/N = 9.7$ dB and RMSE = 8.9%).

Concerning the resolution, the intrinsic resolution depends on the type of used camera (collimator, crystal, photo-multiplier and measurement electronics). Theoretical resolution is determined by the reconstruction method and its algorithm. The inclusion of scattered radiation increases considerably the number of detected photons, and thus would contribute to improve the S/N and the resolution of the imaging system. To evaluate accurately the resolution, it is necessary to have access to real data and to compare it with other methods which do not make use of scattered radiation. At the moment it is too early to use our preliminary results of simulation for this purpose. This work is ongoing with more realistic experimental conditions.

Since our main objective in this article is to show how to exploit advantageously Compton scattered radiation to generate a new imaging principle, we present only results on image formation as well as object reconstruction from scattered rays.

In real situations, of course, one must take into account other factors such as absorption by the medium, Poisson emission noise and the imperfections of the detector (collimator and measuring electronics).

The case of constant mean absorption (often assumed in the literature) is included in our recent work [7]. (The treatment of inhomogeneous absorption poses special mathematical difficulties. Recall that the inversion of the inhomogeneous attenuated X-ray transform in transmission imaging has been just found recently in 2001 [13], despite the fact that the inverse of the Radon transform is known since 1917).

Concerning emission noise there are well known methods to deal with it, such as the method of Maximum Likelihood or the methods of wavelets. They may be used for "denoising" the measured data beforehand or jointly with the inversion process.

As for the imperfections of the detector, the standard way for treating this problem is to make use of a response function of the Gaussian type operating with spatial coordinates as well as with energy coordinate. These issues are discussed in detail in references [1,12].

4. CONCLUSION AND COMMENTS

In this work we have given theoretical results showing the feasibility of object reconstruction using Compton-scattered rays in gamma emission imaging. The new linear integral transform as well as its kernel (SPSF) are derived directly from a Compton-scattering physical analysis [5], which has been strongly recommended to be included in quantitative imaging by experts of the field [6]. The new imaging principle proposed here takes advantage of properties of scattered rays instead of rejecting them as usually done in most actual scatter correction methods. It would improve the signal-to-noise ratio, and consequently the contrast. Moreover, the fact that the angle of scattering is a free parameter is used here as a disposable parameter to collect data, the multi-views of the object are obtained without the need of moving the detector. This possibility is particularly interesting in the applications where the number of measurements is very limited, e.g. in non destructive testing. Several perspectives of the proposed approach are possible: for example extension of this result obtained in emission imaging to transmission imaging and to prospective higher order Compton scattering imaging processes.

NOMENCLATURE

$f(\mathbf{V})$ = object density function
$\tilde{g}(\mathbf{D}, \theta)$ or $g(\mathbf{D}, t)$ = image density function
n_e = electron density in medium
$p(\mathbf{D}, t|\mathbf{V})$ = scatter point spread function
t = tangent of the angle θ, $\tan\theta$
$\mathcal{T}$ = integral transformation
$Y(s)$ = heaviside unit step function
μ = absorption coefficient
θ = Compton scattering angle
2D/3D = two/three-dimensional
S/N = signal-to-noise ratio
RMSE = root mean square error

References

[1] Mai K. Nguyen, C. Faye, L. Eglin and T.T. Truong (2001). Apparent image formation by Compton scattered photons in gamma-ray imaging. *IEEE Signal Processing Letters*, **8**(9), 248.
[2] H.H. Barrett and W. Swindell (1981). *Radiological Imaging I and II*. Academic Press, New York.
[3] B. Davies (2001). *Integral Transforms and their Applications*. Springer, New York.
[4] N.N. Lebedev (1955). *Special Functions and their Applications*. Dover, New York.
[5] Mai K. Nguyen and T.T. Truong (2002). On an integral transform and its inverse in nuclear imaging. *Inverse Problems*, **18**(1), 265.
[6] M.S. Rosenthal, J. Cullom, W. Hawkins, S.C. Moore, B.M.W. Tsui and M. Yester (1995). Quantitative SPECT imaging: a review and recommendations by the focus committee of the society of nuclear medicine computer and instrumentation council. *J. Nucl. Med.*, **36**, 1489.
[7] Mai K. Nguyen and T.T. Truong (2002). Exact inversion of a compounded conical radon transform and a novel nuclear imaging principle. *C.R. Acad. Sci. Paris*, *Ser. I*, **335**, 213.
[8] H. Zaidi (1999). Relevance of accurate Monte Carlo modeling in nuclear medical imaging. *Med. Phys.*, **26**, 574.
[9] S.J. Norton (1994). Compton scattering tomography. *J. Appl. Phys.*, **76**(4), 2007.
[10] M. Singh (1983). An electronically collimated gamma camera for single photon emission computed tomography. *Med. Phys.*, **10**, 421.
[11] M.J. Cree and P.J. Bones (1994). Towards direct reconstruction from a gamma camera based on Compton scattering. *IEEE Trans. Medical Imaging*, **13**(2), 398.
[12] L. Eglin (2002). *Imagerie Scintigraphique: Modélisation et Restauration Multi*-énergétiques. Ph.D Thesis, Université de Cergy-Pontoise.
[13] R. Novikov (2001). Une formule d'inversion pour la transformation d'un rayonnement X atténuie. *C. R. Acad. Sci. Paris*, *Ser. I*, **332**, 1059.
[14] T.T. Truong, Mai K. Nguyen, H.D. Bui and C. Daveau. Determination of the electronic density in a medium by an inverse method based on double-Compton scattering in transmission imaging. *Inverse Problems in Engineering: Theory and Practice*, *volume II*, H.R.B. Orlande (ed.), (E-papers, Rio de Janeiro 2002), 304–412.